The point at which the interference of the variations begins to affect the mod–max occurs when $x_0 - s_2 k = s_2\sigma$. Substituting in for the value of s_2, the cross-over scale for two adjacent smooth variations is

$$s_0 = \sqrt{\left(\frac{x_0}{k+\sigma}\right)^2 - s_1^2}. \tag{5}$$

IV. Conclusion

In this brief, we have investigated the motivation for the isolation assumption of the mod–max method for characterizing signal variations. We found that two motivations exist. First, the mod–max method for characterizing signal variations requires that the wavelet transform mod–max for a particular variation be tracked across scales. Interference from adjacent signal variations may cause the maxima to not be accurately tracked. Second, the method requires that the mod–max being tracked be due to a single variation, not a combination of variations. Interference from an adjacent signal variation may alter the correct maximum.

We have defined "isolated" for discontinuities and smooth variations of one-dimensional signals. In doing so, we formed three classes of isolation for adjacent signal variations: 1) total isolation; 2) semi-isolation; and 3) nonisolation. Total isolation refers to the case where the adjacent signal variations cause no interference. Semi-isolation refers to the case where the adjacent signal variations cause interference, but this interference does not affect the tracking of maxima across scales, which is inherent to the implementation of the mod–max method. Nonisolation refers to the case where the adjacent signal variations cannot be accurately characterized by the mod–max method. These results are summarized in Table I.

References

[1] D. Marr and E. Hildreth, "Theory of edge detection," *Roy. Soc. Lon. Proc.*, vol. 207B, pp. 187–217, 1980.

[2] A. P. Witkin, "Scale space filtering," in *Proc. Int. Joint Conf. Artificial Intell.*, Karlsruhe, Germany, 1983, pp. 1019–1021.

[3] J. Canny, "A computational approach to edge detection," *IEEE Trans. Pattern Anal. Mach. Intell.*, vol. 8, pp. 679–698, Nov. 1986.

[4] S. Mallat and W. L. Hwang, "Singularity detection and processing with wavelets," *IEEE Trans. Info. Theory*, vol. 38, pp. 617–643, Mar. 1992.

[5] S. Mallat and S. Zhong, "Characterization of signals from multiscale edges," *IEEE Trans. Pattern Anal. Machine Intell.*, vol. 14, pp. 710–732, July 1992.

[6] J. Lu, D. M. Healy, Jr., and J. B. Weaver, "Contrast enhancement of medical images using multiscale edge representation," *Opt. Eng.*, vol. 33, no. 7, pp. 2151–2161, July 1994.

[7] L. Velho, D. Terzopoulos, and J. Gomes, "Constructing implicit shape models from boundary data," *Comput. Vis. Image Processing*, vol. 57, no. 3, pp. 220–234, May 1995.

[8] L. M. Bruce, "Multiresolution signal analysis with applications to mammographic lesion classification," Ph.D. dissertation, Dep. Elec. Comput. Eng., Univ. of Alabama, Huntsville, 1996.

[9] L. M. Bruce, R. R. Adhami, and J. W. Bruce, "Appropriate scales when using wavelets for feature extraction," in *Intell. Eng. Syst. Through Artif. Neural Networks, Proc. Artif. Neural Networks Eng.'96*, Dagli *et al.*, Eds., St. Louis, MO, Nov. 1996.

[10] S. Pei and C. Lin, "The detection of dominant points on digital curves by scale-space filtering," *Pattern Recogn.*, vol. 25, no. 11, pp. 1307–1314, Nov. 1992.

[11] P. Wunsch and A. F. Laine, "Wavelet descriptors for multiresolution recognition of handprinted characters," *Pattern Recogn.*, vol. 28, no. 8, pp. 1237–1249, Aug. 1995.

[12] L. M. Bruce and R. R. Adhami, "Wavelet based feature extraction for mammographic lesion recognition," in *Proc. SPIE Int. Symp. Medical Imaging*, Newport Beach, CA, Feb. 1997.

[13] Y. Lu and R. C. Jain, "Behavior of edges in scale space," *IEEE Trans. Pattern Anal. Machine Intell.*, vol. 11, pp. 337–356, 1989.

[14] L. Wu and Z. Xie, "Scaling theorems for zero-crossings," *IEEE Trans. Pattern Anal. Machine Intell.*, vol. 12, pp. 46–54, 1990.

[15] R. Alter-Gartenberg, F. O. Huck, and R. Narayanswamy, "Compact image representation by edge primitives," *CVGIP: Graphical Models Image Processing*, vol. 56, no. 1, pp. 1–7, Jan. 1994.

[16] J. Babaud, A. Witkin, M. Baudin, and R. O. Duda, "Uniqueness of the Gaussian kernel for scale-space filtering," *IEEE Trans. Pattern Anal. Machine Intell.*, vol. 8, pp. 26–33, Jan. 1986.

[17] A. L. Yuille and T. A. Poggio, "Scaling theorems for zero crossings," *IEEE Trans. Pattern Anal. Machine Intell.*, vol. 8, pp. 15–25, Jan. 1986.

Multiscale Edge Detection on Range Images via Normal Changes

Chwen-Jye Sze, Hong-Yuan Mark Liao, Hai-Lung Hung, Kuo-Chin Fan, and Jun-Wei Hsieh

***Abstract*— A new edge detection technique based on detection of normal changes is proposed. Most of the existing range image-based edge detection algorithms base their detection criterion on depth or curvature changes. However, the depth change-based approch does not have keen sensitivity in detecting roof (or crease) edges, and the curvature change-based approach suffers from a complicated and tedious principal curvature derivation process. Using normal changes as a detecting criterion, on the other hand, the existence of an edge can be easily detected, even when the change across a boundary is slight. Experimental results using both synthetic and real images demonstrate that the proposed method can efficiently detect both step and roof edges.**

I. Introduction

Extraction of edges from an image is an important early vision process. It has been of interest to researchers in the area of computer vision from the outset [1]–[3]. The algorithms developed for edge detection can be divided into two categories depending on the type of acquired image. For an intensity image, the devised algorithms usually aim to detect step edges. This is due to the natural limitation of this type of image. For a range image, since the depth information is available, it is possible to correctly detect both step edges and roof edges (or crease edges). In computer vision, since closed contours are more useful for higher level image analysis and since range images can be used to more easily achieve this goal, we shall focus on range image-based edge detection in this brief.

In this brief, we propose a new edge detection technique based on detection of normal changes. The normal value is an important characteristic in differential geometry [4]. We find that by detecting normal changes, both step edges and roof edges can be easily

Manuscript received November 15, 1996; revised November 18, 1997. This work was supported by the National Science Council of Taiwan, , R.O.C., under Grant NSC86-2745-E-001-004.

C.-J. Sze and K.-C. Fan are with the Institute of Computer Science and Information Engineering, National Central University, Chung-Li, Taiwan, R.O.C.

H.-Y. M. Liao is with the Institute of Information Science, Academia Sinica, Nankang, Taipei, Taiwan, R.O.C. (e-mail: liao@iis.sinica.edu.tw).

H.-L. Hung is with the Department of Electrical Engineering and Computer Science, Northwestern University, IL 60208 USA.

J.-W. Hsieh is with Computer and Communication Research Laboratories, Institute of Technology Research Industry, Taiwan, R.O.C.

Publisher Item Identifier S 1057-7130(98)04692-8.

identified. The whole detection procedure is divided into two stages. In the first stage, the normal of every point in a range image is decided. Since all the data points in a range image are discrete, the partial derivatives which are required to derive the normal value cannot be directly computed. For comparison purposes, we propose use of quadratic surface fitting [5], the orthogonal wavelet-based approach [1], and the nonorthogonal wavelet-based approach [2], respectively, to approximate the original object surfaces and then to calculate the normal value of every discrete point on the surfaces. After the normal values of all the surface points are determined, the nonorthogonal wavelet transform (dyadic wavelet transform) proposed by Mallat *et al.* [2] is applied to detect those points which have significant normal changes as edge points. From the experimental results, we find that the nonorthogonal wavelet-based approach can best approximate the original surfaces from a discrete data set. Further, we also find that edge detection based on normal changes is a more promising alternative than other methods that base their detection criterion on depth or curvature changes. The proposed edge detector can detect both step edges and roof edges without introducing any edge models or heuristics.

II. Range Edge Detection via Normal Change

In this section, we shall explain why normal change can be used as a cue for range edge detection. Some properties of a 3-D surface from the differential geometry viewpoint which are useful for edge detection will be addressed in Section II-A. Then, a detailed explanation of why normal change is a better choice for edge detection will be given in Section II-B.

A. Some Properties in Differential Geometry Useful for Edge Detection

In this subsection, some basic properties of a 3-D surface will be addressed from the differential geometry viewpoint. These properties are useful for solving the edge detection problem on range images.

Let $\mathcal{S}$ be a differentiable surface and $\vec{p}(u,v)$ be a point on $\mathcal{S}$ with coordinate (u,v). If $\vec{p}_u$ and $\vec{p}_v$ are the partial derivatives of $\vec{p}(u,v)$ with respect to u and v, respectively, then we can say that $\vec{p}_u$, $\vec{p}_v$ form the basis of a tangent plane, $T(p)$, of $\vec{p}(u,v)$ (Fig. 1). The normal of $T(p)$ can be defined as

$$\vec{N}(u,v) = \frac{\vec{p}_u \times \vec{p}_v}{\|\vec{p}_u \times \vec{p}_v\|}. \tag{1}$$

Here, the norm of any $\vec{N}(u,v)$ is always equal to 1, and all $\vec{N}(u,v)$'s lie on a unit sphere in R^3. The mapping, $\vec{N}: \mathcal{S} \rightarrow R^3$, is called the Gauss mapping, $G(R^3)$ [4].

Let $\vec{N}(u,v)$ be differentiable; the mapping, $d\vec{N}(u,v)$, is from $G(R^3)$ to a tangent plane, $G(R^3)$, at $\vec{N}(u,v)$. Since the tangent plane of $\vec{N}(u,v)$ is equal to that of $\vec{p}(u,v)$, $d\vec{N}(u,v)$ is also on the $T(p)$ plane, as shown in Fig. 1. Thus, both $d\vec{p}$ and $d\vec{N}$ can be represented by the linear combination of du and dv as follows [4]:

$$d\vec{p} = \vec{p}_u\, du + \vec{p}_v\, dv \tag{2}$$

and

$$d\vec{N} = \vec{N}_u\, du + \vec{N}_v\, dv. \tag{3}$$

Here, $p(u,v)$ is the gray level (intensity image) or depth (range image) at position (u,v). Therefore, $d\vec{p}$ physically means the intensity or depth change with respect to $\vec{p}(u,v)$'s neighbors. As for $\vec{N}_u$ and $\vec{N}_v$, they are mathematically defined as $\vec{N}_u = \partial\vec{N}/\partial u$ and $\vec{N}_v = \partial\vec{N}/\partial v$. That is, they physically mean the normal change along the u and v directions, respectively.

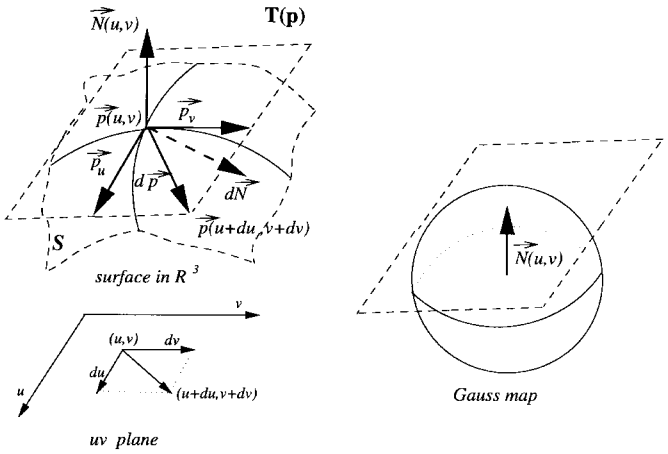

Fig. 1. Relations between a surface point, its corresponding parameter coordinate, and the Gauss map.

B. Why Normal Change is Better for Edge Detection

Equations (2) and (3) represent, respectively, the depth (or intensity) change and the normal change with respect to the neighbors of $p(u,v)$. The drawback of using (2) is that the depth (or intensity) change can only be detected when its value is significant. Since $d\vec{p}$ in (2) cannot be applied to detect different types of edges, we propose use of $d\vec{N}$ [(3)] instead. In what follows, we shall explain why $d\vec{N}$ is chosen to locate broader types of edges. In Fig. 2(a)–(d), four different types of crease(roof) edges, including convex and concave edges, are shown. Fig. 2(e)–(h), respectively, shows the corresponding normal changes across edges. These difference vectors are all normalized and fit into Gaussian spheres. From the normal changes, we find that their values are much more significant than those of the depth (or intensity) changes. Considering a more general case shown in Fig. 2(i), an edge occurs between a plane and a curve surface. It is clear that the normal change between p_2 and p_3 (two points located on different surfaces) is much larger than the normal change between p_4 and p_5 (two points belonging to the same surface) [Fig. 2(j) and (k)]. Therefore, use of the normal change, $d\vec{N}$, instead of the depth (or intensity) change, $d\vec{p}$, is better for finding a more powerful edge detector.

Comparing the normal change-based approach and the curvature-based approach [3], the computational complexity of the former is much less than that of the latter. As shown in Fig. 3, $\{du, dv\}$ and $\{e_1, e_2\}$ are two independent orthonormal bases on the tangent plane of $\vec{p}$. Based on differential geometry, the two principal curvatures, κ_1 and κ_2, can be derived by projecting $d\vec{N}$ on a specific basis. Let $\{e_1, e_2\}$ be the basis with e_1 and e_2 corresponding, respectively, to the directions of the two principal curvatures, κ_1 and κ_2 [4]. From Fig. 3, it is obvious that $d\vec{N}$ can be represented by a linear combination based on either $\{du, dv\}$ or $\{e_1, e_2\}$. One thing to be noted is that no matter how $d\vec{N}$ is represented, its magnitude is independent of the basis selected. The only thing that will vary with respect to the basis change is the orientation of $d\vec{N}$. Therefore, using the normal change directly to locate edge positions does not require that the values of two principal curvatures be explicitely determined. This fact explains why $d\vec{N}$ can replace the two principal curvatures in edge detection and why using $d\vec{N}$ is much more efficient than using κ_1 and κ_2.

III. Calculating Normals from Discrete Surface Points

In the previous section, we have discussed how the change of normals at every point on a surface [(3)] can be used to detect edges. The continuous domain normal value derivation process is

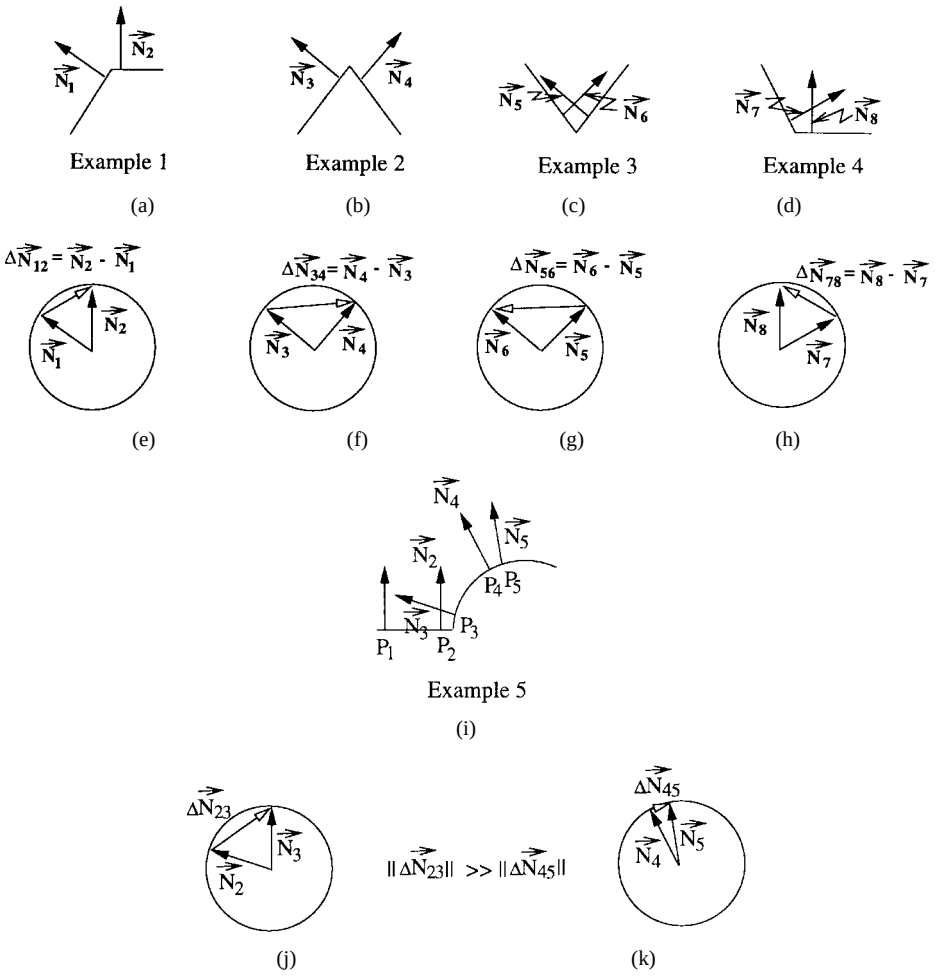

Fig. 2. Five different type of edges and their corresponding Gauss mappings.

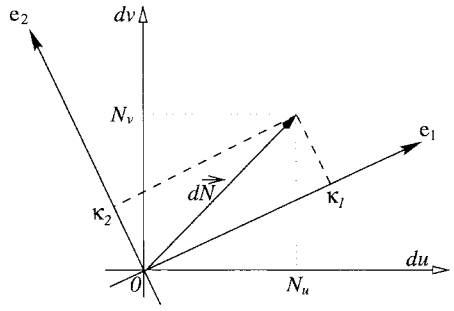

Fig. 3. Relationship between $d\vec{N}$ and principal curvatures.

summarized as follows. Let $\vec{p}(u,v) = (u, v, f(u,v))$ be a point located on a surface. The partial derivatives of $\vec{p}(u,v)$ in the u and v directions are $\vec{p}_u = \partial\vec{p}(u,v)/\partial u = (1 \;\; 0 \;\; f_u(u,v))$ and $\vec{p}_v = \partial\vec{p}(u,v)/\partial v = (0 \;\; 1 \;\; f_v(u,v))$, respectively. Plugging these two values into (1), the value of $\vec{N}(u,v)$ can be rewritten as

$$\vec{N}(u,v) = \left(\frac{-f_u}{\sqrt{1+f_u^2+f_v^2}} \quad \frac{-f_v}{\sqrt{1+f_u^2+f_v^2}} \quad \frac{1}{\sqrt{1+f_u^2+f_v^2}} \right) = (n_1(u,v) \quad n_2(u,v) \quad n_3(u,v)) \tag{4}$$

where $f_u = \partial f(u,v)/\partial u$ and $f_v = \partial f(u,v)/\partial v$, $n_1(u,v) = -f_u/\sqrt{1+f_u^2+f_v^2}$, $n_2(u,v) = -f_v/\sqrt{1+f_u^2+f_v^2}$, and $n_3(u,v) = 1/\sqrt{1+f_u^2+f_v^2}$. The ranges of n_1, n_2, and n_3 are all bounded by $(-1,1)$. In real implementation, since all the data points acquired in a range image are discrete by nature, the above calculation does not apply. Therefore, we have to find an appropriate method to deal with this problem. In the implemenation stage, we split the edge detection procedure into two steps. In the first step, the normal at every point on a surface should be determined. This step involves calculation of partial derivatives on a set of discrete data points. Then, in the second step, a detector is required to accurately detect the points where significant variations of normals are encountered. In order to calculate the normals on a set of discrete surface points, some existing methods [2], [5] can be applied. For comparison purposes, we choose quadratic surface fitting [5], the orthogonal wavelet-based approach [6], and the nonorthogonal wavelet-based approach [2] to calculate the normal value of every point on a surface.

IV. Detecting Edges Based on Normal Changes

In [2], Mallat and his students developed some pioneering works for multiscale edge detection based on gray level changes. Here, we shall review part of their work which will be useful in our work. Define two wavelet functions, $\psi^1(x,y)$ and $\psi^2(x,y)$ [2], where

$$\psi^1(x,y) = \frac{\partial\theta(x,y)}{\partial x} \tag{5}$$

and

$$\psi^2(x,y) = \frac{\partial\theta(x,y)}{\partial y}. \tag{6}$$

$\theta(x,y)$ is a smoothing function whose integration over the full domain is equal to 1 and converges to 0 at infinity. These two functions have to satisfy the following conditions:

$$\int_{-\infty}^{\infty}\int_{-\infty}^{\infty}\psi^1(x,y)\,dx\,dy = 0 \tag{7}$$

and

$$\int_{-\infty}^{\infty}\int_{-\infty}^{\infty}\psi^2(x,y)\,dx\,dy = 0. \tag{8}$$

Let $f(x,y) \in \boldsymbol{L}^2(\boldsymbol{R})$. The so-called dyadic wavelet transform [2] of $f(x,y)$ at scale 2^j along the x and y directions can be represented, respectively, by

$$W^1_{2^j}f(x,y) = f * \psi^1_{2^j}(x,y) \tag{9}$$

and

$$W^2_{2^j}f(x,y) = f * \psi^2_{2^j}(x,y) \tag{10}$$

where $\psi^1_{2^j}(x,y) = (1/2^{2j})\psi^1(x/2^j, y/2^j)$ and $\psi^2_{2^j}(x,y) = (1/2^{2j})\psi^2(x/2^j, y/2^j)$. In what follows, we shall use the above mentioned dyadic wavelet transform to detect significant normal changes as edge points.

From (3), it is obvious that the vector of the normal change, $d\vec{N}(u,v)$, can be represented by the linear combination of the two bases on the du–dv plane, i.e., $N_u\,du + N_v\,dv$. Also, their associated weights are the gradients of $\vec{N}$ along the du and dv directions, respectively. Since the dyadic wavelet transform proposed by Mallat [2] can be used to calculate the magnitudes of these gradients, we can apply their method directly to calculate $d\vec{N}(u,v)$. According to the formulation reported in [2], the vector dyadic wavelet transform of $\vec{N}(u,v)$ at scale 2^j can be defined as follows:

$$\mathcal{W}_j\vec{N}(u,v) = W^1_{2^j}\vec{N}(u,v)\,du + W^2_{2^j}\vec{N}(u,v)\,dv \tag{11}$$

where

$$W^1_{2^j}\vec{N}(u,v) = \left(W^1_{2^j}n_1(u,v),\quad W^1_{2^j}n_2(u,v),\quad W^1_{2^j}n_3(u,v)\right) \tag{12}$$

and

$$W^2_{2^j}\vec{N}(u,v) = \left(W^2_{2^j}n_1(u,v),\quad W^2_{2^j}n_2(u,v),\quad W^2_{2^j}n_3(u,v)\right). \tag{13}$$

Since the $\mathcal{W}_j\vec{N}(u,v)$ vector also lies on the du–dv plane, the magnitude and argument of $\mathcal{W}_j\vec{N}(u,v)$ can be directly computed. Referring to [2], the norms of $W^1_{2^j}\vec{N}(u,v)$ and $W^2_{2^j}\vec{N}(u,v)$ should be defined, respectively, as follows:

$$\left\|W^1_{2^j}\vec{N}(u,v)\right\| = \sqrt{\left[W^1_{2^j}n_1(u,v)\right]^2 + \left[W^1_{2^j}n_2(u,v)\right]^2 + \left[W^1_{2^j}n_3(u,v)\right]^2} \tag{14}$$

and

$$\left\|W^2_{2^j}\vec{N}(u,v)\right\| = \sqrt{\left[W^2_{2^j}n_1(u,v)\right]^2 + \left[W^2_{2^j}n_2(u,v)\right]^2 + \left[W^2_{2^j}n_3(u,v)\right]^2}. \tag{15}$$

The magnitude of $\mathcal{W}_j\vec{N}(u,v)$ at scale 2^j can, thus, be computed as follows:

$$M_{2^j}\vec{N}(u,v) = \sqrt{\left[\left\|W^1_{2^j}\vec{N}(u,v)\right\|\right]^2 + \left[\left\|W^2_{2^j}\vec{N}(u,v)\right\|\right]^2}. \tag{16}$$

Furthermore, the angle of $\mathcal{W}_j\vec{N}(u,v)$ with respect to du direction is

$$A_{2^j}\vec{N}(u,v) = \text{argument}\left(\left\|W^1_{2^j}\vec{N}(u,v)\right\| + i\left\|W^2_{2^j}\vec{N}(u,v)\right\|\right). \tag{17}$$

From the above calculations, every point in a range image will obtain two values. One is the magnitude of its normal change with respect to its neighbors, and the other is the direction tendency of this point. Like other multiscale edge detection methods [2], [7], the edge points can be determined by locating those local extrema whose normal changes exceed a preset threshold.

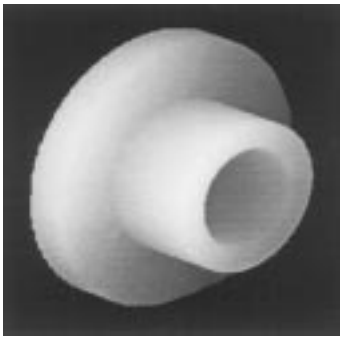

Fig. 4. A synthetic range image: agpart.

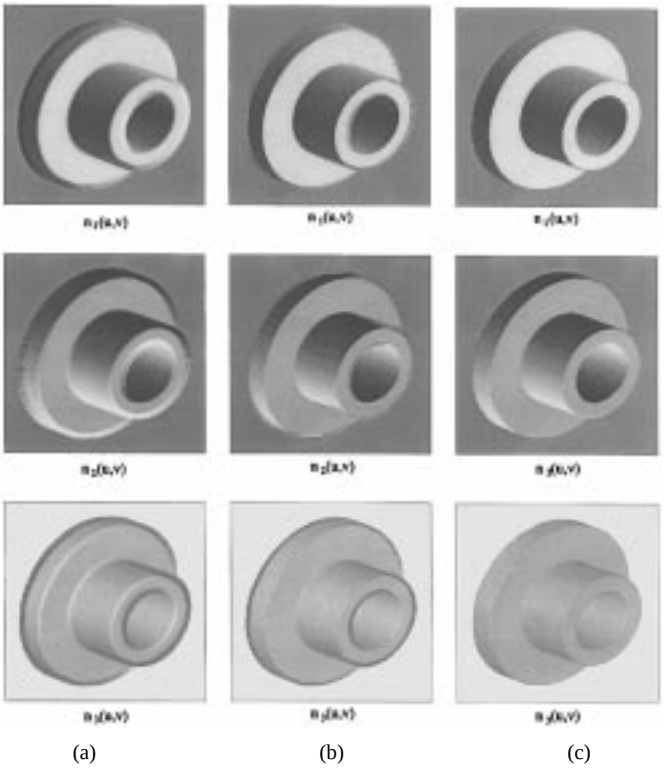

(a) (b) (c)

Fig. 5. Three component of normals (n_1, n_2, n_3) estimated by using (a) quadratic surface fitting, (b) the orthogonal wavelet-based approach with three vanishing moments, and (c) the nonorthogonal wavelet-based approach.

V. Experimental Results

In the experiments, a number of synthetic and real range images were adopted as test images to corroborate the effectiveness of the proposed method. Fig. 4 showed a synthetic image: agpart. The size of the agpart image was 240×240. We also used three real images with different sizes.

In the first stage of the experiment, the normal of every point in a range image had to be decided. In order to make a comparison, we used three different methods, i.e., quadradic surface fitting, and orthogonal and nonorthogonal wavelet-based approaches, to calculate the normal values. For this part we used the synthetic image, "agpart," as the test image. The experimental results of this part are shown in Fig. 5. Fig. 5(a) shows the three normal components (n_1, n_2, n_3) detected by applying the quadratic surface fitting method. Fig. 5(b) and

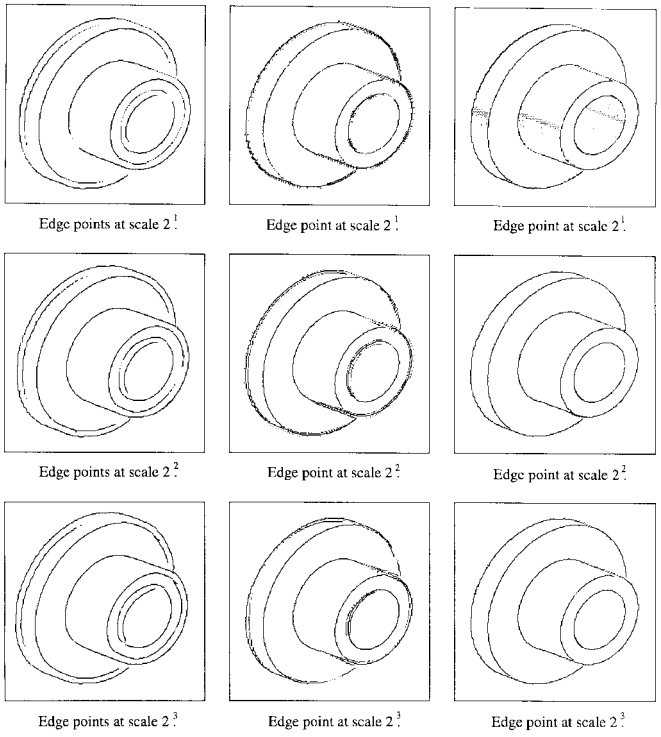

Fig. 6. Detected edge points at different scales using (a) quadratic surface fitting, (b) the orthogonal wavelet-based approach with three vanishing moments, and (c) the nonorthogonal wavelet-based approach.

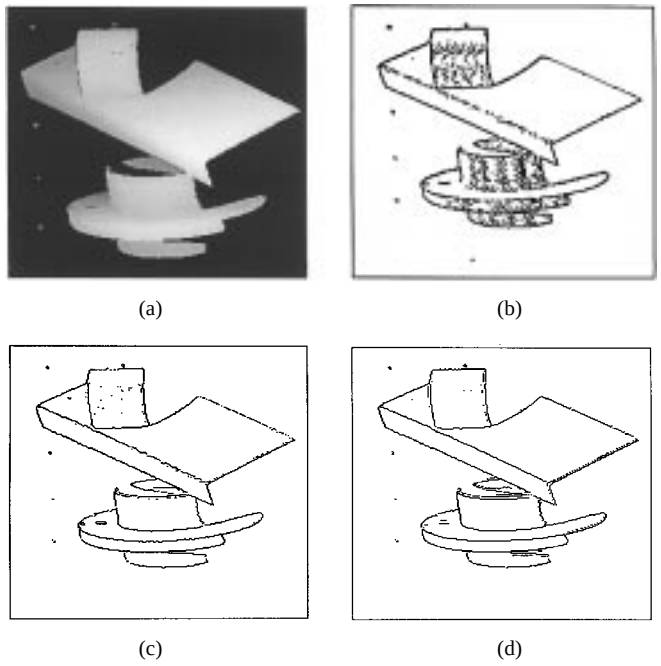

Fig. 7. Detected edge points at different scales from real image "occl."

(c) show, respectively, the normal components obtained by applying the orthogonal (Daubechies' wavelets with three vanishing moments) and the nonorthogonal (Mallat–Zhong's wavelet) approaches.

Based on the derived normals, we then used the vector dyadic wavelet transform (11), the dyadic wavelet transform proposed by Mallat *et al.* [2], to calculate the normal change of every point in an

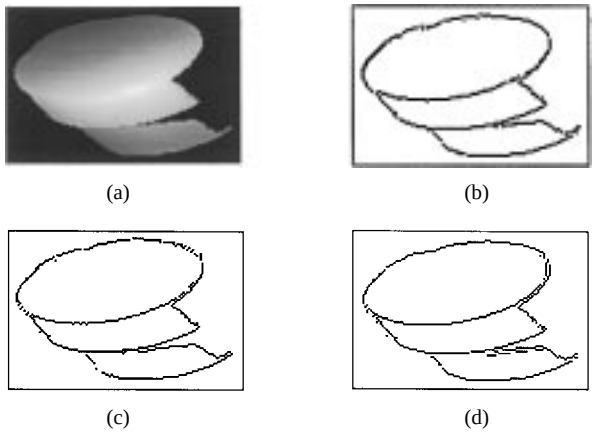

Fig. 8. Detected edge points at different scales from real image "adapter."

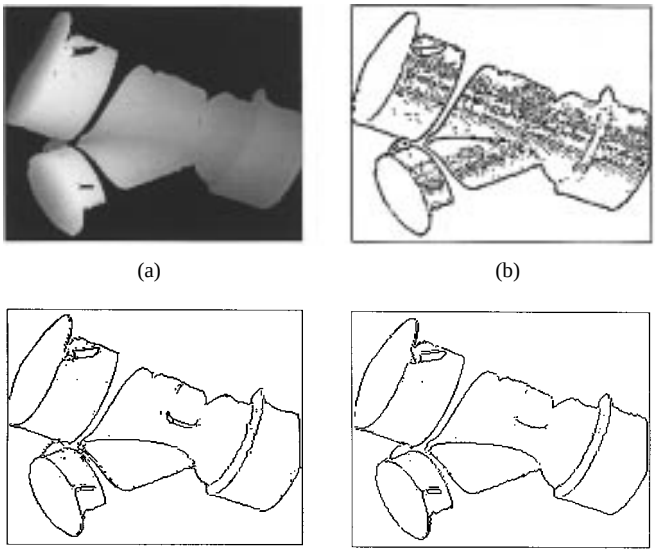

Fig. 9. Detected edge points at different scales from real image "bigwye."

image and selected those local extrema as edge points. Fig. 6(a)–(c) shows, respectively, the multiscale edges ($2^1, 2^2$, and 2^3) detected from three differently approximated surfaces. Among them, Fig. 6(a) shows the multiscale edges detected from the normals obtained using the quadratic surface fitting method. Fig. 6(b) and (c) show the multiscale edges detected when the approximation method was the orthogonal approach and nonorthogonal approach, respectively. It is apparent that, when the quadratic surface fitting or the orthogonal wavelet-based approach was adopted to estimate the normal values, the detected edges contained some spurious results or the original edges delocalized from their original position. On the other hand, the edges detected from the normals as estimated by the nonorthogonal wavelet-based approach were the best results.

One thing to be noted is that the first stage of the proposed approach, i.e., the normal determination step, is crucial because a "poor" estimation of normal values may have an irrecoverable effect on the edge detection stage. A poor estimation method may smooth out the original image and, thus, delocalize edges from their correct locations. After comparing the empirical results, the nonorthogonal wavelet-based approximation was chosen because it produced the best results out of the three methods. Figs. 7 and 8 show the results of

a sequence of experiments based on real range images. All of these results were obtained by applying the nonorthogonal wavelet-based approach to estimate the normal values. From the results, we can find that most of the crease (roof) edges were detected correctly.

VI. Conclusion and Discussion

In this brief, we have proposed a new edge detection technique based on detection of normal changes. We have found that, by detecting normal changes, both step edges and roof edges can be easily identified. Therefore, the new technique has been proven to be a more promising method than other methods that base their detection criterion on depth or curvature changes. The whole detection procedure is divided into two stages. In the first stage, the normal of every point is decided. Since these data points are discrete, we have proposed use of three different approximation techniques to approximate the original surfaces. Based on the approximated continuous surfaces, the normals of all the points on the surfaces can be computed. Then, we applied the dyadic wavelet transforms to calculate the normal change value of every point on the surfaces. Finally, the edge points could be determined by locating those local extrema whose normal change values exceeded a preset threshold. Experimental results using both synthetic and real images have demonstrated that the proposed method is indeed superb in detecting both step and roof (or crease) edges in a range image.

References

[1] J. W. Hsieh, M. T. Ko, H. Y. Mark Liao, and K. C. Fan, "A new wavelet-based edge detector via constrained optimization," *Image Vision Computing*, vol. 15, pp. 511–527, 1997.

[2] S. Mallat and S. Zhong, "Characterization of signal from multi-scale edges," *IEEE Trans. Pattern Anal. Machine Intell.*, vol. 14, no. 7, pp. 710–732, July 1992.

[3] O. Monga and S. Benayoun, "Using partial derivatives of 3D images to extract typical surface features," *Computer Vision Image Understanding*, vol. 61, no. 2, pp. 171–189, Mar. 1995.

[4] M. P. Do. Carmo, *Differential Geometry of Curves and Surfaces.* Englewood Cliffs, NJ: Prentice-Hall, 1976.

[5] P. J. Besl and R. C. Jain, "Invariant surface characteristics for three-dimensional object recognition in range images," *CVGIP*, vol. 33, pp. 33–80, 1986.

[6] J. W. Hsieh, H. Y. M. Liao, M. T. Ko, and K. C. Fan, "Wavelet-based shape from shading," *Graphical Models Image Processing*, vol. 57, no. 4, pp. 343–362, July 1995.

[7] J. W. Hsieh, H. Y. M. Liao, M. T. Ko, K. C. Fan, and Y. P. Hung, "Image registration using an edge-based approach," *Computer Vision Image Understanding*, vol. 67, no. 2, pp. 112–130, Aug. 1997.

Pyramid-Based Multiresolution Adaptive Filters for Additive and Multiplicative Image Noise

Bruno Aiazzi, Luciano Alparone, Stefano Baronti, and Giorgio Borri

***Abstract*— In this brief, adaptive filtering is applied to the different resolutions of the Laplacian pyramid of a noisy image. For natural images, each layer is characterized by an SNR that increases as resolution decreases. Therefore, each filter may be adjusted to achieve adaptivity also across scales. Theoretical frameworks are developed for *signal-dependent* noise models. A *rational* Laplacian pyramid is employed to handle multiplicative noise. Experiments carried out on gray-level images corrupted by true and simulated noise, show the potentiality of the approach compared to other established algorithms, in terms both of SNR improvements and of enhancement in visual quality.**

***Index Terms*— Image processing, Laplacian pyramid, local statistics filtering, speckle noise.**

I. Introduction

A general approach to image noise reduction is based on modeling: multiplicative and generally *signal-dependent* models are widely used to describe the noise introduced by several imaging systems [1]. Stationarity hypotheses are usually made on the noise, but are seldom satisfied by the signal. Thus, filters that exploit both local statistics and geometric features perform better. In this light, adaptive filtering is the key to edge-preserving image smoothing. A crucial point, however, is determining the pixel neighborhood, in which the parameters driving the smoothing algorithm are to be estimated. A first approach consists of adaptively modifying the shape and/or size of the local processing window at each pixel position, based on some local feature (e.g., mean, variance, edges), thereby determining the filter response in the presence of such characteristics [2], [3]. An equivalent approach that has been only recently formalized is considering a multiresolution decomposition of the input image obtained by applying a different nonlinear adaptive filter to each resolution layer [4]. The wavelet decomposition has been employed for multiresolution denoising, thanks to its capability to capture spatial features within frequency subbands [5]. However, wavelet decompositions are *critically sampled* (i.e., *nonredundant*) image descriptions, viz., the image may be exactly synthesized from a number of coefficients as large as the number of pixels. This property implies that connected spatial structures analyzed at increasing resolutions are split into separate sub-bands, thereby losing their spatial connectivity. On the contrary, Laplacian pyramids (LP) [6], [7] which are *oversampled* (i.e., *redundant*) image decompositions, look attractive because of their *band-pass* frequency property, which enables connected image structures to be represented onto multiple scales.

In this work, an established adaptive filter [1] is applied to the connectivity-preserving different resolution layers in which the noisy image is decomposed by an LP-generating procedure. For naturally

Manuscript received November 30, 1996; revised December 15, 1997. This work was supported in part by grants of the Italian Space Agency (ASI).

B. Aiazzi and S. Baronti are with the Nello Carrara Research Institute on Electromagnetic Waves, IROE-CNR, I-50127 Florence, Italy.

L. Alparone is with the Department of Electronic Engineering, University of Florence, I-50139 Florence, Italy.

G. Borri is with CERN, Geneva, Switzerland, on leave from the Department of Electronic Engineering, University of Florence, I-50139 Florence, Italy.

Publisher Item Identifier S 1057-7130(98)04677-1.